Hamiltonian nontwist map for magnetic field lines with locally reversed shear in toroidal geometry

R. Balescu
Association Euratom-Etat Belge pour la Fusion, Université Libre de Bruxelles, Code Postal 231, Campus Plaine, Boulevard du Triomphe, B-1050 Bruxelles, Belgium
(Received 21 April 1998)

A simple Hamiltonian map is constructed, fulfilling the minimum requirements for the representation of a tokamak magnetic field in reversed shear configuration. This ''revtokamap'' is a typical nontwist map, for which many theorems of ''traditional'' dynamical systems theory do not apply. It is shown that in the revtokamap, for finite stochasticity parameter, a critical surface appears, separating an external, globally stochastic region from a robust nonstochastic core region. This phenomenon of ''semiglobal chaos'' is analogous to the well-known appearance of an internal transport barrier in reversed shear tokamak experiments. An analysis of the fixed points reveals a variety of bifurcation and reconnection phenomena, which appear to be generic for nontwist maps with an impenetrable polar axis. [S1063-651X(98)09809-2]

PACS number(s): 52.25.Fi, 05.45.+b, 52.25.Gj

I. INTRODUCTION

In a previous work [1] we constructed an iterative map, called a *tokamap*, representing a model of the magnetic field lines in a toroidally confined plasma, such as in a tokamak configuration. Such a map generates phase portraits of possibly chaotic orbits in a much simpler way than the direct integration of the field line differential equations. It is well known that the latter have a Hamiltonian form in which the toroidal flux coordinate ψ (divided by B_0a^2) and the poloidal angle coordinate θ (divided by 2π) play respective roles of canonically conjugate momentum and position variables, the toroidal angle ζ (divided by 2π) plays the role of time, and the poloidal flux $\alpha(\psi,\theta,\zeta)$ (scaled by B_0a^2) is the Hamiltonian. (Here B_0 is a characteristic magnetic field intensity, and a is the minor radius of the torus). It is, in general, impossible to construct a map that is *exactly equivalent* to a given Hamiltonian system without solving the equations of motion (which is precisely what one wants to avoid). One wishes to construct, instead, a model *ab initio*, and check its relevance *a posteriori*. A map representing a global picture of a tokamak cross section perpendicular to the magnetic axis should satisfy at least two important constraints:

(i) The map should be Hamiltonian (or symplectic), hence area preserving. This implies [2,3] that the coordinates $(\psi_{\nu+1},\theta_{\nu+1})$ at ''time'' $\nu+1$ be related to the coordinates (ψ_ν,θ_ν) at ''time'' ν by a canonical transformation (here ν is an integer).

(ii) The map must be *compatible with toroidal geometry*. This implies that the radial coordinate ψ be a definite positive number. In particular, if at time zero $\psi_0>0$, then at all later times ν, $\psi_\nu>0$; and if $\psi_0=0$, then $\psi_\nu=0$ for all ν. Thus the polar axis must be an impenetrable barrier.

It was shown in Ref. [1] that the following map satisfies the constraints

$$\psi_{\nu+1}=\psi_\nu-\frac{K}{2\pi}\frac{\psi_{\nu+1}}{1+\psi_{\nu+1}}\sin 2\pi\theta_\nu, \tag{1}$$

$$\theta_{\nu+1}=\theta_\nu+W(\psi_{\nu+1})-\frac{K}{(2\pi)^2}\frac{1}{(1+\psi_{\nu+1})^2}\cos 2\pi\theta_\nu. \tag{2}$$

Here K is a real number called the *stochasticity parameter*; its range of physical interest is $0\leqslant K\leqslant 2\pi$. $W(\psi)$ is the unperturbed *winding number* [or the inverse safety factor, $1/q(\psi)$]: its role will be thoroughly discussed below. Relation (1) is made explicit by solving for $\psi_{\nu+1}$ and keeping only the positive root:

$$\psi_{\nu+1}=\tfrac{1}{2}\{P(\psi_\nu,\theta_\nu)+\sqrt{[P(\psi_\nu,\theta_\nu)]^2+4\psi_\nu}\}, \tag{3}$$

where the function $P(\psi,\theta)$ is defined as

$$P(\psi,\theta)=\psi-1-\frac{K}{2\pi}\sin 2\pi\theta. \tag{4}$$

The map defined by Eqs. (1)–(4) is called the Tokamap. It was shown that it reproduces qualitatively many global features of the magnetic configurations found in tokamak experiments.

The winding number profile $W(\psi)$ determines the properties of the phase portrait in an essential way. In Ref. [1] a class of Tokamaps was studied, corresponding to ''classical'' experiments in which $W(\psi)$ is a monotonously decreasing function of ψ [hence $q(\psi)$ is a monotonously increasing function]. In ''tokamak terminology,'' this is expressed by saying that the *shear* $s=[\psi/q(\psi)]dq(\psi)/d\psi$ is definite positive over the whole range of the radial coordinate. In ''dynamical systems language,'' this means that these tokamaps are *twist maps*.

In recent years an important amount of work, both experimental and theoretical, has been devoted to tokamak situations with a locally reversed shear (see, e.g., Refs. [4–12] and further references therein). In these experiments, the safety factor profile has a local minimum; hence the $W(\psi)$ function is no longer a monotonously decreasing function, but rather possesses a maximum. The main importance of such *reversed shear configurations* for controlled fusion re-

 © 1998 The American Physical Society

sults from the formation of an *internal transport barrier* (apparently first mentioned in Ref. [4]). The radial transport in the central region is thus significantly reduced, the core being efficiently insulated from the outside. As a result, the temperature and density profiles have a very flat section in the core, followed by an abrupt drop near the edge (this feature is particularly visible in the experiments described in Refs. [11,12]). Because of these favorable phenomena, the reversed shear appears as an essential ingredient of the so-called ''advanced tokamak scenarios'' [13]). Theoretical work has been concentrated on mechanisms of stabilization of some instabilities by the effect of shear (trapped particle modes, $\mathbf{E}\times\mathbf{B}$ velocity shear effects, etc.). It will be shown here that the tokamap reproduces the formation of a magnetic field configuration that strikingly suggests the presence of a transport barrier. The (cautious) interpretation of this fact will be discussed below.

The implementation of a reversed shear profile into the tokamap is very easy: one simply chooses for $W(\psi)$ an appropriate function which has a maximum at some value of ψ between 0 and 1. The resulting map then becomes a typical nontwist map. Such maps have not been very extensively studied in the past: in particular, most textbooks on dynamical systems do not mention them, because some of the ''great'' theorems (such as the Kolmogorov-Arnold-Moser theorem) are not valid for them. A very clear early study of simple maps of this type is the work by Howards and Hohs [14]. Various aspects of nontwist maps were studied in Refs. [15–17]. The most extensive existing studies of nontwist maps are found in a series of papers by del-Castillo-Negrete and co-workers [18–21]. In these works the paradigm called the *standard nontwist map* is analyzed in great detail. Because of its apparent simplicity, this map plays the same role as the Chirikov-Taylor standard map for twist maps. It is defined as follows:

$$y_{n+1}=y_n-b\,\sin(2\pi x_n),\quad x_{n+1}=x_n+W_S(y_{n+1}),\quad (5)$$

with

$$W_S(y)=a(1-y^q). \quad (6)$$

Here a and b are real numbers and, typically, $q=2$. The domain of interest in this problem is: $-\infty<y<\infty$, and $-\frac{1}{2}<x<\frac{1}{2}(\mathrm{mod}\ 1)$.

The simplicity of this map makes it possible to study in depth its mathematical properties, using, in particular, methods based on the renormalization group, in order to analyze the transition to chaos. From the tokamak point of view, however, this map has the same drawbacks as the standard map. In particular, y cannot be interpreted as a radial coordinate, because it takes both positive and negative values.

In order to model a reversed shear experiment in a tokamak, we use the tokamap, Eqs. (1)–(3), in which we introduce a winding number function $W(\psi)$ that adequately represents a reversed shear profile. We thus produce a Hamiltonian map which satisfies the geometrical constraints defined above, and is a typical non-twist map. For brevity, we call such a nontwist map a Revtokamap. (From here on, for the sake of brevity, we denote by *tokamap* a map [Eqs. (1)–(3)] with a *monotonous winding number profile*.) The price to be paid is the higher complexity of the revtokamap, compared to the standard nontwist map. As far as we can see at present, this precludes, for instance, the use of such elegant methods as the renormalization group for the study of the transition to chaos.

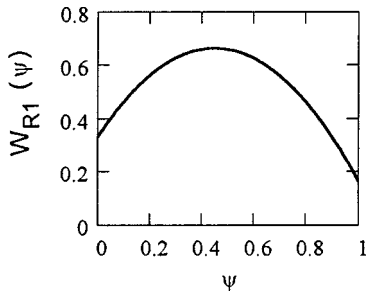

FIG. 1. Unperturbed revtokamap winding number profile $W_{R1}(\psi)$.

II. GLOBAL PROPERTIES OF THE REVTOKAMAP

There is considerable freedom in the choice of the profiles. In order to study the structure of the revtokamap we consider a simple class of W profiles of the following form:

$$W_R(\psi)=w[1-a(c\psi-1)^2]. \quad (7)$$

This function depends on three parameters. In order to improve the physical insight, we express the latter in terms of the following quantities: w, the maximum value of W_R; w_0, the value of W_R on the axis $[w_0=W_R(0)]$; and w_1, the value of W_R at the edge $[w_1=W_R(1)]$. We then obtain

$$a=\frac{w-w_0}{w},\quad c=1+\left(\frac{w-w_1}{w-w_0}\right)^{1/2}. \quad (8)$$

The maximum of W is located at the radial position

$$\psi_M=\left[1+\left(\frac{w-w_1}{w-w_0}\right)^{1/2}\right]^{-1}. \quad (9)$$

A first set of parameters is chosen as follows:

$$W_{R1}\begin{cases} w_0=0.3333 \\ w=0.6667 \\ w_1=0.1667. \end{cases} \quad (10)$$

The resulting profile (Fig. 1) fits rather closely the experimental data recently published by the DIIID team [9].

We first consider the *unperturbed revtokamap*, Eqs. (1) and (2), with $K=0$ and $W(\psi)\rightarrow W_{R1}(\psi)$. In Fig. 2 we show a typical phase portrait of the unperturbed revtokamap corresponding to this profile. Compared to the corresponding portrait for the tokamap (see Fig. 1 or Ref. [1]), we note the following features.

(i) All periodic orbits (starting at $\theta=0$) of winding number $W>w$ are absent from the phase portrait. In particular, *there is no fixed point* $(W=1)$ in this case.

(ii) The periodic orbits (starting at $\theta=0$) with winding numbers in the range $w_0<W<w$ appear in pairs (i.e., there are two such orbits, located at different values of ψ).

(iii) The periodic orbits (starting at $\theta=0$) with winding numbers $w_1<W<w_0$ are single (like in the tokamap).

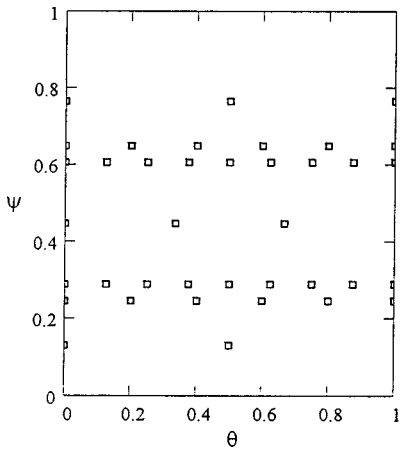

FIG. 2. Unperturbed revtokamap phase portrait [profile: $W_{R1}(\psi)$].

(iv) The same statements hold, of course, also for *KAM* barriers. We note, in particular, that there are *two golden KAM barriers* ($W=g_*=0.61803\ldots$), sandwiched between the periodic orbits $W=\frac{3}{5}$ and $\frac{5}{8}$.

In Fig. 3 we show a revtokamap phase portrait showing five orbits (the number of iterations is $N=1000$), for a small value of the stochasticity parameter $K=0.8$. Nothing spectacular appears here. The periodic orbits generate island chains, whereas irrational winding numbers produce *KAM* barriers. Let us recall that the real winding number in a perturbed map of form (1) is no longer given by the function $W_R(\psi)$, but rather must be estimated directly from the definition

$$\omega=\lim_{\nu\to\infty}\frac{\Theta_\nu-\theta_0}{\nu}, \tag{11}$$

where Θ_ν is the lift of the angle θ_ν, (i.e., its value calculated without the prescription ''mod 1''). As a result, it appears that the winding number $\omega=\frac{2}{3}$ is no longer attained for $K\neq 0$: the maximum appears to be $\omega\approx 0.66639\ldots$ (for $K=0.8$). This being an irrational number, there is no three-island chain in the middle of the diagram [evolving from the period-3 orbit for $W_R(0.44949)=\frac{2}{3}$ in the unperturbed case of Fig. 2]. There instead appears a *KAM* barrier at this maximum winding number. Although it is not a straight line parallel to the θ axis, it plays the role of a kind of ''symmetry axis.'' The winding numbers corresponding to successive *KAM* barriers or islands decrease upon moving downward

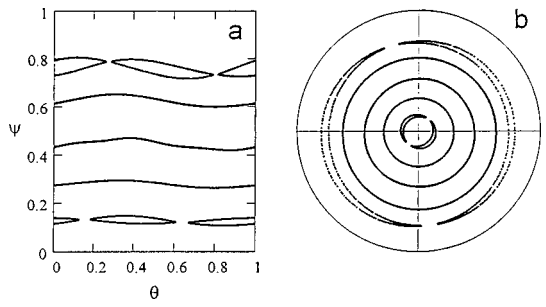

FIG. 3. Revtokamap phase portrait $K=0.8$ [profile: $W_{R1}(\psi)$; $N=1000$].

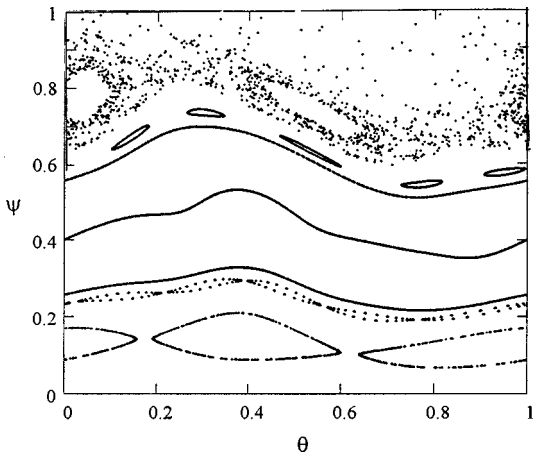

FIG. 4. Revtokamap phase portrait $K=2.8$ [profile: $W_{R1}(\psi)$; $N=3500$].

below this ''axis,'' and are also decreasing upon moving upward above it. It is also interesting to note that the unperturbed period-3 orbits (on the lower branch) with winding number $\omega=\frac{1}{3}$, lying *on the polar axis* do not generate any island chain. This is another special feature of the invariant polar axis in the revtokamap. We again underline the absence of any fixed point in the present case.

These pictures could convey the message that a nontwist map roughly behaves like two ''halves'' of a tokamap put together, each of them being the image of the other in a ''mirror'' located at the maximum of the winding number profile. Such a statement is valid only for small values of the stochasticity parameter. (It will be seen below, however, that some very peculiar phenomena may occur in the revtokamap even at very small values of K.)

Figure 4 represents a phase portrait of the revtokamap for $K=2.8$, a rather moderate value: for the monotonous tokamap, there is no global chaos for this value of K. The following features appear in this case.

(i) The *symmetry axis* is rather strongly distorted.

(ii) In a certain strip around this ''symmetry axis,'' the phase portrait is similar to the previous one: *KAM* barriers and islands come in ''symmetric'' pairs below and above the axis. In Fig. 4, two ''golden'' *KAM* barriers $\omega=g_*$, and the two five-island chains with $\omega=\frac{3}{5}$, are visible. These islands are very nicely shaped: the chaotic layers around them are so thin that they cannot be seen in this picture. The whole region within and below this strip is almost perfectly regular (i.e., nonchaotic).

(iii) The most conspicuous feature is seen in the upper part of the phase portrait, which is invaded by a chaotic orbit. Within this chaotic region some structure can be seen (as usual): thus a two-island chain mirroring the lower $\omega=\frac{1}{2}$ islands is clearly visible. On the other hand, only a few of the 3500 points of the chaotic orbit depicted here are visible. The reason for this is that most iterates of the starting point ($\psi_0=0.8$, $\theta_0=0.2$) wander out of the physical region into the region, $\psi>1$. Thus *in the upper part of the revtokamap phase space the chaos is global*. On the other hand, *this chaotic region is very sharply bounded below by a KAM barrier*. In the present example we find that the bounding *KAM* shown in Fig. 4 corresponds to $\omega\approx 0.5772$. We note, in passing, that this barrier lies well above the golden *KAM*

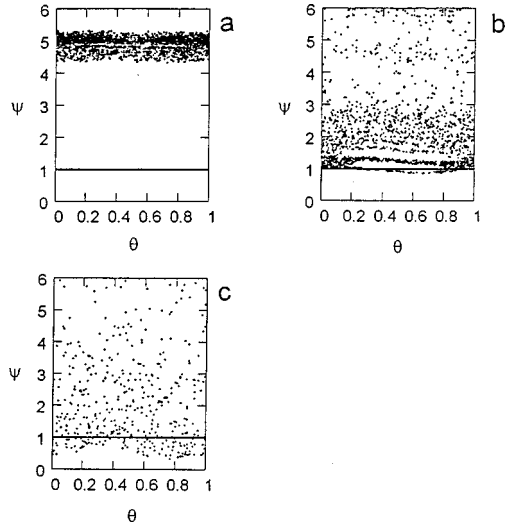

FIG. 5. Typical chaotic revtokamap orbit in the extended phase space ($N=2300$). (a) $K=0.25$. (b) $K=1.4$. (c) $K=6.3$.

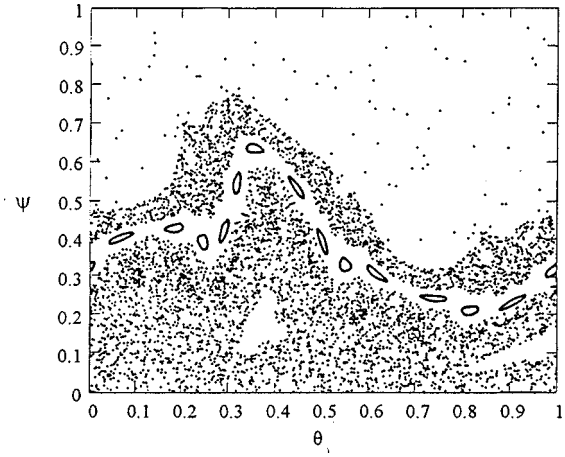

FIG. 6. Two chaotic orbits separated by an island chain. $K=6.3$ ($N=3500$).

surface. Thus there appears within the physical domain a barrier, sharply separating a *regular core region* from a *globally stochastic edge region*. We are tempted to call this a transport barrier.

The concept of a transport barrier in reversed shear configurations has been very widely discussed in the recent literature [4–13] (see also Ref. [12] in which many papers are devoted to this problem). It has been clearly defined in Ref. [4] as ''a localized region within the plasma where the thermal and particle transport are much smaller than in the surrounding regions.'' I would rather define the transport barrier as the *surface* separating regions of low and high transport. Its occurrence has been related to specific plasmadynamical mechanisms by the authors quoted above. Here I wish to be very prudent in my statements. In the revtokamap model there is no *explicit* treatment of the charged particles. The magnetic field configuration is *static*: it is produced, however, by an underlying distribution of currents in the plasma. It appears, nevertheless, that the mere consideration of this magnetic field configuration gives rise to a similar phenomenon. The nonlinearity of the Hamiltonian revtokamap, combined with a reversed shear profile, produces a transport barrier within the physical region, for a stochasticity parameter larger than some threshold: $K>K_T$. The precise relation of this phenomenon to the plasma transport barrier found in experiments has to be considered more closely in forthcoming work; I cannot believe, however, that this is a mere accident.

The threshold value K_T cannot be defined very precisely. We suggest the following procedure. Consider the revtokamap *extended above the physical range*, $\psi>1$. We note that even for very small values of K there is a ''ghost'' transport barrier in the unphysical range [Fig. 5(a)]. As K increases, the transport barrier moves downwards. We define the threshold K_T as the value of K for which the transport barrier enters the physical domain: with the present parameters, we find $K\approx 1.4$ [Fig. 5(b)]. The definition is not very sharp, because the barrier is not a straight horizontal line, but rather a somewhat complicated curve. For K beyond this value, we reach a situation like in Fig. 4, with a core region insulated from the edge by the transport barrier. As K increases further [e.g., $K=6.3$, Fig. 5(c)], the core region begins to develop localized chaotic belts. Nevertheless, for quite a range of K, the two (upper and lower) chaotic regions remain separated from each other by a remnant of the transport barrier. This can be seen in Fig. 6 (a magnified picture of the physical region), which shows a lower chaotic region separated from the upper one by a regular 14-island chain with $\omega \approx 0.642\,83$ ($\approx \frac{9}{14}$).

To sum up, the previous results show an unexpected property of the revtokamap, which can be called *semiglobal chaos*. Even for very small values of the stochasticity parameter there appears a semi-infinite globally chaotic region bounded below by a *KAM* barrier. Above that barrier the orbits extend chaotically without limits towards large ψ, whereas below that barrier the orbits are regular (*KAM* barriers or island chains surrounded by thin stochastic layers). The critical barrier is located in the unphysical region $\psi>1$ for small K, and moves downward with increasing K, until it reaches the limit $\psi=1$ of the physical region. For $K>K_T$, the *transport barrier* separates the physical domain into two parts: the upper one is globally stochastic, whereas the lower one remains regular up to rather large values of K. The two regions remain insulated from each other over a wide range of K, even when the lower one becomes chaotic.

It is very interesting to note that a phenomenon quite similar to a transport barrier was found in Ref. [15]. These authors studied a one-dimensional strongly driven anharmonic oscillator, described by a Hamiltonian $H=\frac{1}{2}p^2+x^q+\beta x\cos\tau$, (where β is the stochasticity parameter and $q>2$ is a positive parameter). In their system, [after transformation to action and angle variables (J,φ)] the winding number profile presents a *minimum* at a finite value of J. For a sufficiently large value of the coupling parameter, a semiglobal chaotic regime is visible in the Poincaré section (obtained by numerical integration of the continuous time differential equations). The arrangement is, however, opposite of the one appearing in the revtokamap (Figs. 4 and 5): a transport barrier separates a *core region* that is *chaotic*, from an *edge region* that is *regular* (Fig. 6 of Ref. [15]). The core region thus acts as a *chaotic trap*. This result clearly shows the complementary behaviors of nontwist maps with winding number profiles having a maximum and profiles having a

minimum. The important point is that semiglobal chaotic behavior seems to be a generic property of nontwist maps originating from very different physical problems.

III. FIXED POINT ANALYSIS

It was shown in Ref. [1] that a number of interesting bifurcations appear in the (positive shear) tokamap when the control parameters K and/or w are varied. In the revtokamap, bifurcation phenomena occur which are characteristic of nontwist maps, but are also due to the invariance of the polar axis. Some of these nontwist map phenomena were first studied in Refs. [14] and [18–21].

We start our considerations with an analysis of the *fixed points* of the revtokamap. As we know from Sec. II, fixed points do not always exist. In order to study the problem quantitatively, we write down the equations determining the fixed points by using Eqs. (1) and (2) with $\psi_{\nu+1}=\psi_\nu=\psi$ and $\theta_{\nu+1}=\theta_\nu=\theta$:

$$\frac{\psi}{1+\psi}\sin 2\pi\theta=0, \tag{12}$$

$$W(\psi)-\frac{K}{(2\pi)^2}\frac{1}{(1+\psi)^2}\cos 2\pi\theta=0 \pmod 1. \tag{13}$$

The study of fixed points should be completed by a *linear stability* analysis, based on the calculation of the *residue* $R_R=\frac{1}{4}(2-\mathrm{Tr}\,M)$, (where M is the matrix defining the tangent map) [22–25]. The form of the residue is very similar to Eq. (44) of Ref. [1], with $W(\psi)\to W_R(\psi)$:

$$R_R=-\frac{K}{8\pi}\left\{\left[\frac{1}{(1+\psi)^2}-\frac{2\pi}{2\pi(1+\psi)^2+K\sin 2\pi\theta}\right]\sin 2\pi\theta-\frac{K}{\pi}\frac{\psi}{(1+\psi)^4}\cos^2 2\pi\theta+4\pi Kwac(c\psi-1)\frac{\psi}{1+\psi}\cos 2\pi\theta\right\}, \tag{14}$$

where a and c are defined by Eqs. (8). The fixed point (around which the map is linearized) is linearly stable (O point), whenever $0\leqslant R_R\leqslant 1$, otherwise it is an unstable X point. We look for solutions of Eqs. (12) and (13) in the physical domain: $0\leqslant\psi\leqslant 1$ and $0\leqslant\theta\leqslant 1$, with $0\leqslant K\leqslant 2\pi$.

Equation (12) has a first class of solutions, like in the tokamap, for $\psi=0$, corresponding to fixed points on the polar axis. Equation (13) then reduces to

$$G_R(\theta,K,n;w_0)\equiv w_0-\frac{K}{(2\pi)^2}\cos 2\pi\theta-n=0, \tag{15}$$

where the definition $w_0=W(0)$ was used; n is an arbitrary integer. This equation has the obvious solution

$$\cos 2\pi\theta=\frac{(2\pi)^2}{K}(w_0-n). \tag{16}$$

This solution is real iff

$$n-\frac{K}{(2\pi)^2}\leqslant w_0\leqslant n+\frac{K}{(2\pi)^2}. \tag{17}$$

This condition only involves the winding number on axis, w_0; additional constraints must, however, be satisfied. We first note that zero or negative values are excluded for the unperturbed winding number W. A vanishing W would correspond to an infinite q, and this value cannot be crossed. Hence, we must assume

$$w_0>0, \quad w>0, \quad w_1>0. \tag{18}$$

On the other hand, w being (by definition) a maximum, we have the two obvious conditions:

$$w_0<w, \quad w_1<w. \tag{19}$$

Consider first the case $n=0$. Combining Eqs. (17)–(19), we find that there exists a real solution of Eq. (16) for

$$0<w_0\leqslant\min\left(\frac{K}{(2\pi)^2},w\right). \tag{20}$$

We note that within the physical range of the stochasticity parameter, $K/(2\pi)^2$ is a very small number. Hence, even when $w>K/(2\pi)^2$, the restriction $w_0<K/(2\pi)^2$ is physically uninteresting. An analogous discussion of the case $n\geqslant 2$ also leads to the conclusion that w and w_0 would be restricted to physically irrelevant (too large) values.

The physically relevant case is thus $n=1$. In this case we define a minimum and a maximum threshold, just as in the tokamap case, Eq. (55) of Ref. [1]:

$$w_m=1-\frac{K}{(2\pi)^2}, \quad w_M=1+\frac{K}{(2\pi)^2}. \tag{21}$$

In the revtokamap, we identify three possibilities.

(a) When

$$w\geqslant w_M, \tag{22}$$

a real solution for the fixed point exists whenever

$$w_m\leqslant w_0\leqslant w_M. \tag{23}$$

(b) When

$$w_m\leqslant w\leqslant w_M, \tag{24}$$

a real solution for the fixed point exists whenever

$$w_m\leqslant w_0\leqslant w. \tag{25}$$

(c) When

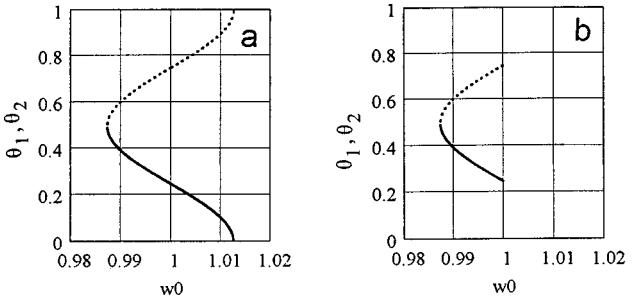

FIG. 7. Angular position of the fixed points X_1 and X_2 on the polar axis. $K=0.5$. (a) $w=1.2$. (b) $w=1$.

$$w<1-\frac{K}{(2\pi)^2}=w_m, \tag{26}$$

there exists no real solution for the fixed point on the polar axis. It therefore appears that the number and type of fixed points on the polar axis is determined by the relative values of w_0 and of w. The value of w_1 is not relevant here, as long as it remains below w_0. The case $w_1>w_0$ appears to be physically uninteresting. Therefore, in the present discussion the value of w_1 is fixed once for all: w_1 *will not be considered as a variable control parameter*.

Case (a) is very similar to the tokamap situation. The discussion of Ref. [1] can be transposed here by replacing the tokamap parameter w by the revtokamap parameter w_0. For given K, and fixed $w>w_M$, there exist two fixed points on the polar axis, in a limited window of values of w_0. Equation (14) shows that the corresponding residues are negative, hence both fixed points are X points. Consider a scan of the parameter space, by starting at some value $w_0<w_m$ and progressively increasing this parameter. At first there is no fixed point on axis. When $w_0=w_m$, there suddenly appears a double fixed point at $\theta=\frac{1}{2}$. When w_0 is further increased, the latter splits into two fixed points which move apart until they merge at $\theta=0$ $(=1 \bmod 1)$ for $w_0=w_M$. For higher values of w_0 the fixed points disappear. w_m and w_M are thus *bifurcation points*, associated with the appearance or disappearance of fixed points. This case is illustrated for the following choice of parameters:

$$K=0.5, \quad w_m=0.987\,33, \quad w_M=1.012\,67. \tag{27}$$

For case (a) we take $w=1.2>w_M$. We also fix the value of $w_1=0.166\,67$ in all the forthcoming figures. The θ values of the two X points are shown in Fig. 7(a). For case (b), we choose $w=1<w_M$. The fixed points start again together at $\theta=0.5$, then move apart for increasing w_0. In order to satisfy condition (19), however, the scan must stop at $\theta_1=0.25$ and $\theta_2=0.75$, for $w_0=1(=w)$ [Fig. 7(b)]. Above this value $(w_0>w)$ the winding number profile no longer has a maximum, and hence the revtokamap reduces to a monotonous tokamap. Note, however, that $w_0=w$ is not a bifurcation point: the X points on axis also exist in a tokamap, as shown in Ref. [1]. Finally, in case (c) there is no fixed point at all on the polar axis. The consequences of this behavior will be discussed below, after the analysis of the other fixed points.

We now discuss the second set of fixed points in the revtokamap, arising from Eqs. (12) and (13) with $\psi\neq 0$. Equation (12) then requires $\sin 2\pi\theta=0$, with the solutions $\theta=\frac{1}{2}$ and $\theta=0$. Substituting these values into Eq. (13), we find

$$\theta=\tfrac{1}{2}: \quad F_1(\psi;K,w_0,w;n)\equiv W_R(\psi)+\frac{K}{(2\pi)^2(1+\psi)^2}-n=0, \tag{28}$$

$$\theta=0: \quad F_2(\psi;K,w_0,w;n)\equiv W_R(\psi)-\frac{K}{(2\pi)^2(1+\psi)^2}-n=0, \tag{29}$$

The number and nature of the solutions of these equations depends on the relative values of the parameters K, w, w_0, and n (we recall that w_1 is fixed once for all). For simplicity, we restrict our discussion to a range of values of the maximum, w, close to $w=1$, which are realistic for a tokamak. The extension to higher or smaller values can easily be done (as in Ref. [1]).

We start our analysis by fixing the value of $K=0.5$ as before. This also determines the values of the thresholds w_m and w_M as in Eq. (27). A graphical visualization is obtained by plotting (numerically) the curves $F_1(\psi)$ and $F_2(\psi)$. It is seen (Fig. 8) that both curves possess a maximum, and hence each of them may intersect the ψ axis in two points. [$F_1(\psi)$ has a singularity at $\psi=-1$, and hence it produces a third zero, which is, however, always negative, and hence unphysical]. The discussion amounts to determining the number and location of the zeroes belonging to the physical domain $0\leqslant\psi\leqslant 1$, for different values of w_0, w, and n. The discussion is guided by the position of the first two parameters with respect to the already known bifurcation points w_m and w_M. The sequence of Fig. 8 shows three typical situations.

We first note that in all three cases, only the choice $n=1$ may produce zeros in the physical domain. By varying the parameters, the curves $n=0,2,3,\ldots$ may also produce ''physical'' roots, but they would correspond to physically irrelevant values of w_0 and w, and will not be further discussed. We thus henceforth *fix the value* $n=1$. Figure 8 illustrates three characteristic cases.

(a) $w_0<w_m$, $w<w_m$. In this case none of the curves F_1 and F_2 (for $n=1$) intersect the ψ axis: the revtokamap has no fixed points at all.

(b) $w_0<w_m$, $w>w_M$. In this case, each one of the functions F_1 and F_2 has two zeros in the physical domain, and hence the revtokamap has four fixed points. The fixed points generated by F_1 are denoted as Y_{11} $(\psi_{11},\theta_{11}=0.5)$ and Y_{12} $(\psi_{12},\theta_{12}=0.5)$, with $\psi_{11}<\psi_{12}$. The fixed points generated by F_2 are denoted as Y_{21} $(\psi_{21},\theta_{21}=0)$, and Y_{22} $(\psi_{22},\theta_{22}=0)$, with $\psi_{21}<\psi_{22}$. The evaluation of the corresponding residues shows that Y_{11} and Y_{22} are X points, whereas Y_{12} and Y_{21} are O points.

(c) $w_0>w_M$, $w>w_M$. Each of the functions F_1 and F_2 possesses a single zero in the physical domain, because the coordinates ψ_{11} and ψ_{21} are negative in this case. The revtokamap now possesses two fixed points in the physical range: an O point Y_{12} and an X point Y_{22}. Although the fixed points Y_{11} and Y_{21} are unphysical (and hence invisible in a polar plot, and inaccessible from the physical region), their

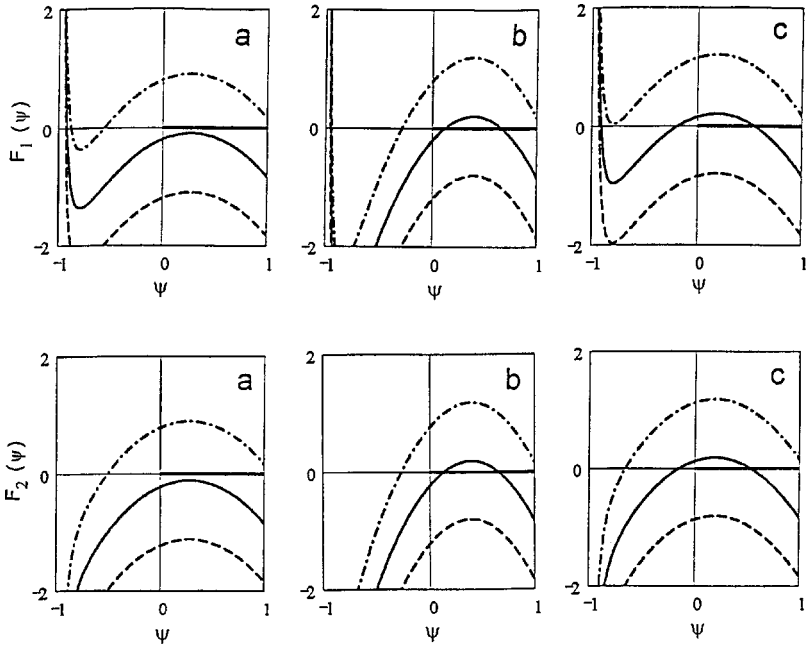

FIG. 8. The curves F_1 and F_2 vs ψ for $K=0.5$. From top to bottom: $n=0$ (dash-dotted line), $n=1$ (solid line), $n=2$ (dashed line). (a) $w_0<w_m$, $w<w_m$ ($w_0=0.8$, $w=0.9$). (b) $w_0<w_m$, $w>w_M$ ($w_0=0.8$, $w=1.2$). (c) $w_0>w_M$, $w>w_M$ ($w_0=1.15$, $w=1.2$).

formal inclusion in the discussion is useful for a clear understanding of the phase space structure, as will be shown in Sec. IV.

The three cases considered above correspond to situations where both parameters w_0 and w lie outside the domain $[w_m, w_M]$. A rich variety of bifurcation phenomena occur when w_0 and/or w enter the latter domain. The variety is due to the fact that the zeros of the functions F_1 and F_2 (see Fig. 8) do not cross the physical border $\psi=0$ simultaneously.

Thus, for instance, for $w>w_M$, when w_0 crosses the lower bifurcation point w_m (i.e., $w_m<w_0<w_M$), the former X point Y_{11} crosses the border ($\psi_{11}<0$) and becomes an O point; simultaneously (as shown above) there appear two X points on the polar axis. In this situation the revtokamap has three X points and three O points, one of which is unphysical.

If, on the other hand, w_0 is kept fixed ($w_0<w_m$), we would (naively) expect a bifurcation when w crosses w_M from above. This is, however, not the case (although an interesting phenomenon occurs at this point, as shown in Sec. IV). The bifurcation occurs at a slightly lower value w_B, through a merging of the O point Y_{21} and the X point Y_{22}, followed by their disappearance for $w<w_B$. There exists thus a third bifurcation point w_B located between w_m and w_M. Its position depends on the value of w_0, and can unfortunately not be expressed analytically.

The various possibilities have been considered systematically (for given K) by successively fixing w inside or outside one of the intervals determined by the ''landmarks'' (w_m, w_B, w_M) and varying w_0. The result of this investigation is given in Table I. In this table, the symbols $[O]$ and $[X]$ characterize the stability of the fixed points; a sign $(+)$ denotes a positive value of ψ (i.e., a physical fixed point), a sign $(-)$ denotes a negative value of ψ (i.e., an unphysical fixed point), and a symbol ''No'' denotes the absence of the corresponding fixed point.

Note that in all cases the Poincaré-Bertrand theorem is satisfied, i.e., there is an equal number of O points and X points, *provided that both physical and unphysical points are taken into account*. This fact was already noted in the case of the Tokamap [1].

The next natural question is what happens when the stochasticity parameter is varied. The only role of K in this respect is to determine the values of w_m and w_M [Eq. (21)] (and also of w_B), without changing their relative positions. Thus a change of K will simply produce a change in the width of the intervals bounded by the three bifurcation points. As a result, *the results of Table I are valid for all K*.

IV. BIFURCATIONS AND RECONNECTIONS IN THE REVTOKAMAP

We now illustrate the various types of bifurcations derived in Sec. III by exhibiting phase portraits corresponding to the various situations described in Table I. We first show several phase portraits ($N=600$) of the revtokamap for fixed $K=0.5$ in various situations. The choice of this relatively small value of K is justified as follows. For this value of K the island chains are still quite well defined, and the phenomena are clearly visible. For larger values of K the classification of Table I remains valid, but thicker stochastic layers build up around the islands, making the visualization of the phenomena less clear.

In case IA ($w>w_M, w_0<w_m$) there are two fixed O points and two fixed X points in the physical domain (Fig. 9). This configuration represents a typical *heteroclinical topology*: the separatrix of each island has two branches, each one joining one X point to the next (in a portrait continued periodically in θ.) When w_0 increases, the lower island progressively moves downward, but is squeezed against the impenetrable polar axis. When $w_0=w_m$, the X point Y_{11} reaches $\psi=0$ and merges with the two X points X_1 and X_2 which

TABLE I. Fixed points of the revtokamap.

		$\psi=0$	$\theta=0$		$\theta=0.5$	
		$X1,X2$	$Y21$	$Y22$	$Y11$	$Y12$
				$w>w_M$		
I A	$w_0<w_m$	No	$[O]+$	$[X]+$	$[X]+$	$[O]+$
I B	$w_m<w_0<w_B$	$[X],[X]$	$[O]+$	$[X]+$	$[O]-$	$[O]+$
I C	$w_B<w_0<w_M$	$[X],[X]$	$[O]+$	$[X]+$	$[O]-$	$[O]+$
I D	$w_M<w_0$	No	$[X]-$	$[X]+$	$[O]-$	$[O]+$
				$w_B<w<w_M$		
II A	$w_0<w_m$	No	$[O]+$	$[X]+$	$[X]+$	$[O]+$
II B	$w_m<w_0<w_B$	$[X],[X]$	$[O]+$	$[X]+$	$[O]-$	$[O]+$
II C	$w_B<w_0<w_M$	$[X],[X]$	$[O]+$	$[X]+$	$[O]-$	$[O]+$
				$w_m<w<w_B$		
III A	$w_0<w_m$	No	No	No	$[X]+$	$[O]+$
III B	$w_m<w_0<w_B$	$[X],[X]$	No	No	$[O]-$	$[O]+$
				$w<w_m$		
IV A	$w_0<w_m$	No	No	No	No	No

appear at this moment [Fig. 10(a)]. Just above the bifurcation, the latter X points are separated, and a ''ghost'' O point appears in the unphysical region [Fig. 10(b)]: we are now in the situation IB of Table I. In the terminology of Ref. [1], the bifurcation produces a decay of the X point Y_{11} into two X points and an O point, with conservation of the stability index (equal to the number of O points minus number of X points). Note that the bifurcation is accompanied by a *reconnection* of the separatrices around the islands centered on Y_{11} and Y_{21}; the topology remains, however, heteroclinic. As w_0 is further increased, the size of the physical island around Y_{21} decreases. The crossing of w_B produces no bifurcation, but, as w_0 reaches w_M, [Fig. 10(c)] the latter island disappears, as well as the two X points X_1 and X_2. This second bifurcation thus produces a ''recombination'' of two X points and an O point, producing a new X point in the unphysical region [Fig. 10(d)]. This type of bifurcation occurs also in the Tokamap [1]. During this sequence of bifurcations, the upper island around Y_{12} (not shown in Fig. 10) remains almost unaffected. One therefore ends up, after the passage of w_0 through the ''bifurcation belt,'' in situation ID of Table I (Fig. 11). A single fixed O point is left in the physical domain: its former ''companion'' has disappeared (because it has moved into the unphysical domain.)

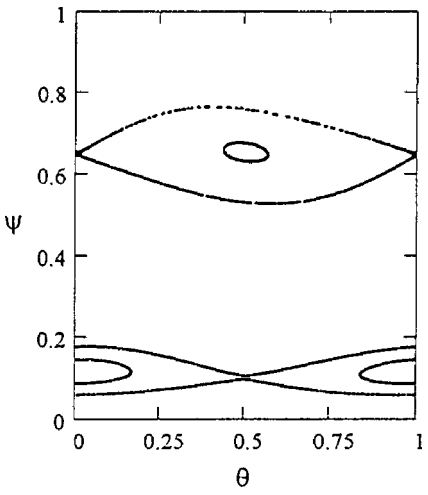

FIG. 9. The two one-island chains, heteroclinic topology, case IA: $w>w_M$, $w_0<w_m$ ($w_0=0.8$, $w=1.2$).

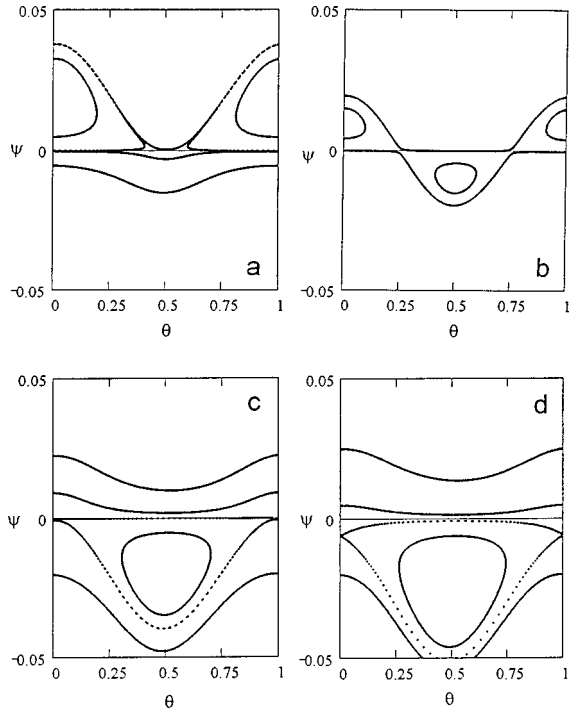

FIG. 10. Disappearance of fixed points by passage through two bifurcations (extended phase space). Fixed: $w>w_M$ ($w=1.2$). (a) First bifurcation: $w_0=w_m$ ($w_0=0.987\,33$). (b) Case IB: $w_m<w_0<w_B$ ($w_0=1$). (c) Second bifurcation: $w_0=w_M$ ($w_0=1.012\,67$). (d) Case ID: $w_0>w_M$ ($w_0=1.2$).

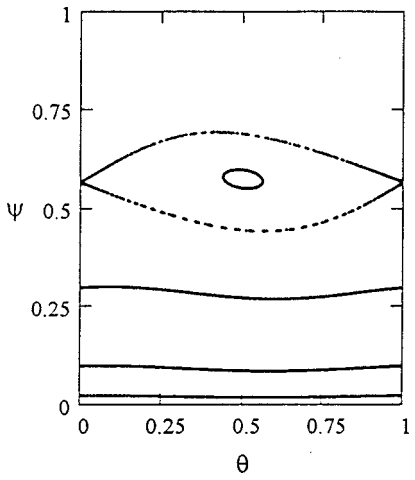

FIG. 11. Single one-island chain in the physical domain, case ID: $w>w_M$, $w_0>w_M$ ($w_0=1.1$, $w=1.2$).

Case III ($w_m<w<w_B$) is very interesting because it exhibits quite a different topology. In this case, the function F_2 has no roots, hence only F_1 produces fixed points. When $w_0<w_m$ (case IIIA), there is an O point and an X point, aligned at the same value of $\theta=0.5$ [Fig. 12(a)]. This gives rise to a *homoclinic topology*, in which the separatrix starting from the X point returns to the same point. For increasing w_0, a bifurcation occurs at $w_0=w_m$, when the X point reaches the polar axis and merges with the newly born X points [Fig. 12(b)]. The bifurcation produces a decay of the X point Y_{11} into two X points and a ghost O point (case IIIB). The structure of the islands in the extended phase space [Fig. 12(c)] is particularly interesting. It displays two O points aligned on $\theta=0.5$ encircled by islands, and two X points on the polar axis. This type of structure was called a ''dipole structure'' by del-Castillo-Negrete and co-workers [18–21]. Here, however, it appears as a ''ghost dipole,'' because one of the islands is located in the unphysical region and the X points are on the polar axis. Hence, in reality (i.e., in the polar representation), only the upper island is visible.

We consider next a different type of scan, keeping w_0 fixed ($w_0<w_m$) and starting at $w>w_M$, case IA, with two island chains in heteroclinic configuration [Fig. 13(a)]. w is now lowered, until it reaches $w=w_M$. There is *no bifurcation* at this point: there are still two O points and two X points; but the upper separatrix touches the lower X point at $\theta=\frac{1}{2}$. This produces *a reconnection* of the two separatrices and a *reorganization into a homoclinic topology* [Fig. 13(b)]. A remarkable fact is that *this process, which involves an overlap of island chains, does not produce chaotization*. This reconnection leading to a change of topology without bifurcation and without chaotization is a characteristic property of nontwist maps, first described by Howard and Hohs [14] and also by del-Castillo-Negrete and co-workers [19–21]. Upon further lowering of w, the size of the island around Y_{21} decreases until, at $w=w_B$, the O point Y_{21} and the X point Y_{22} merge. As a result of this bifurcation, this island disappears: we are in case IIIA [Fig. 13(c)]. When w further decreases, the unique remaining island shrinks while moving very little downward. When w crosses the second bifurcation point w_m, the O point merges with the X point and the island disappears ''on the spot'' [Fig. 13(d)]. Below this threshold there are no fixed points left in the revtokamap (case IVA).

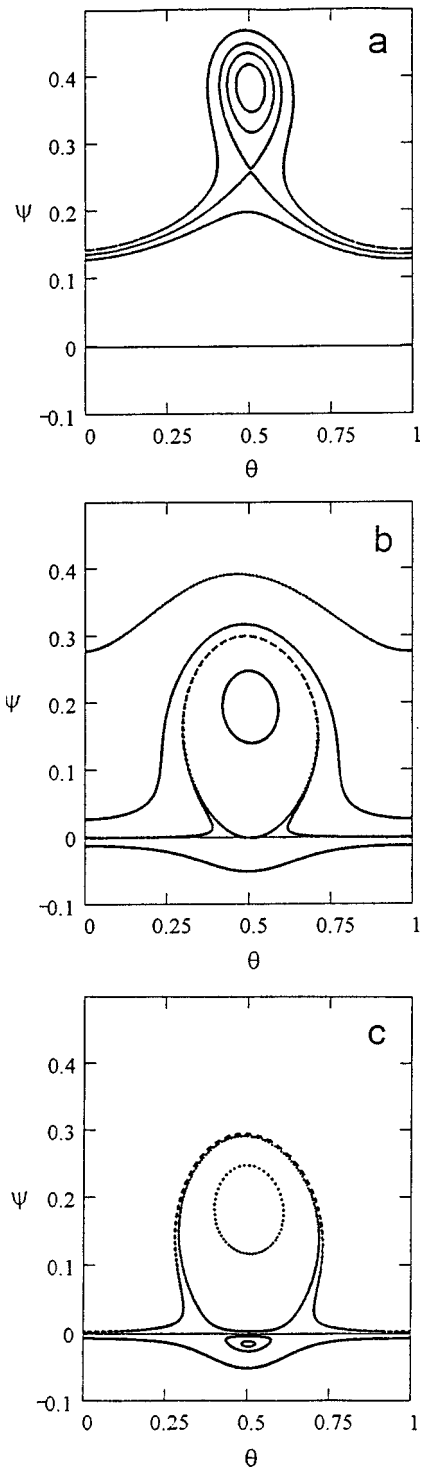

FIG. 12. Dipole formation, homoclinic topology, by passage through a bifurcation (extended phase space). Fixed w: $w_m<w<w_B$ ($w=1$). (a) Single one-island chain, homoclinic, case IIIA: $w_0<w_m$ ($w_0=0.8$). (b) Bifurcation: $w_0=w_m$ ($w=0.987\,33$). (c) Dipole (''ghost''), case IIIB: $w_m<w_0<w_B$ ($w_0=0.99$).

To sum up these results, we have seen that the revtokamap presents a rich variety of bifurcations leading to very different phase portraits. Some of them are of the same nature as in the standard nontwist map, but there are additional types in the revtokamap, due to the presence of the impenetrable polar axis.

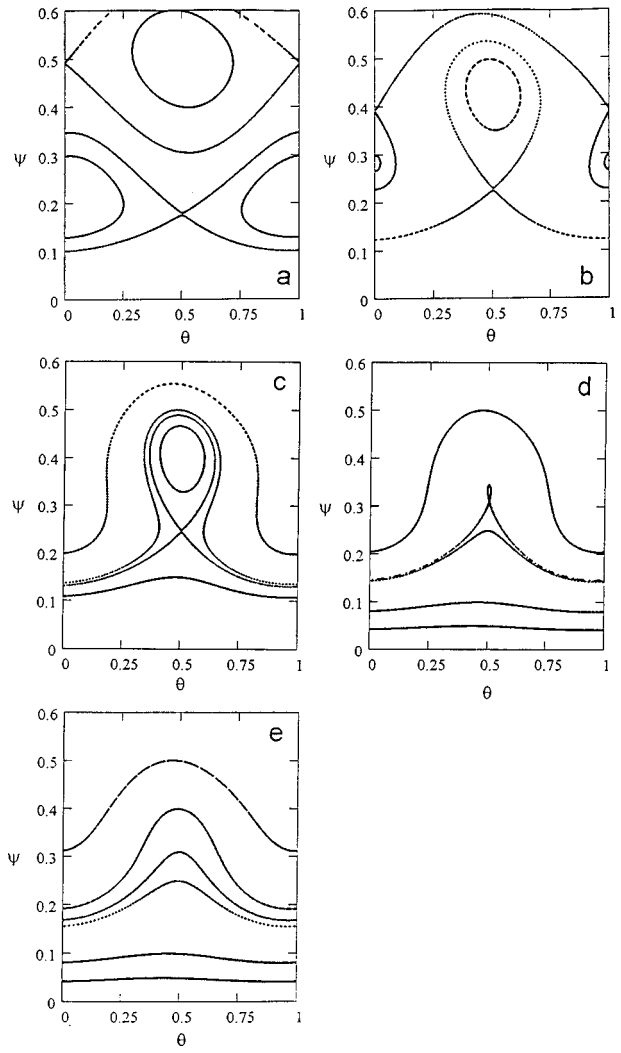

FIG. 13. Separatrix reconnection and disappearance of fixed points in homoclinic topology, by passage through two bifurcations. Fixed: $w_0 < w_m$ ($w_0 = 0.8$). (a) Above reconnection (case IA): $w > w_M$ ($w = 1.05$). (b) At reconnection: $w = w_M$ ($w = 1.012\,67$). (c) Below first bifurcation (case IIIA): $w_m < w < w_B$ ($w = 1.005$). (d) Just above second bifurcation: $w \gtrsim w_m$ ($w = 0.993$). (e) Below second bifurcation (case IVA): $w < w_m$ ($w = 0.98$).

The last point we wish to discuss in this section is the phenomenon of *collision of periodic orbits*. This phenomenon was also first exhibited in Refs. [14] and [18–21] in the standard nontwist map; its appearance is very similar in the revtokamap. For a clear visualization, we now consider a sequence of phase portraits of the revtokamap for *fixed values of w and* w_0. For convenience, we choose $w = 0.67$ and $w_0 = 0.3333$ ($w_1 = 0.166\,67$, as before). We study the evolution of the pair of island chains corresponding to winding number $\omega = \frac{2}{3}$ for varying K. We start at $K = 1.5$: the two island chains have heteroclinic topology, and are located rather close to each other [Fig. 14(a)]. As K increases, the two island chains move closer together until a critical value of K is reached: a process of separatrix reconnection happens at this point, with a transition to homoclinic topology [Fig. 14(b)]. This reconnection is similar to the one of Fig. 13(b). Let us stress again that the overlapping of island chains does not produce chaos. Such nondestructive overlapping is produced when islands corresponding to *different branches of*

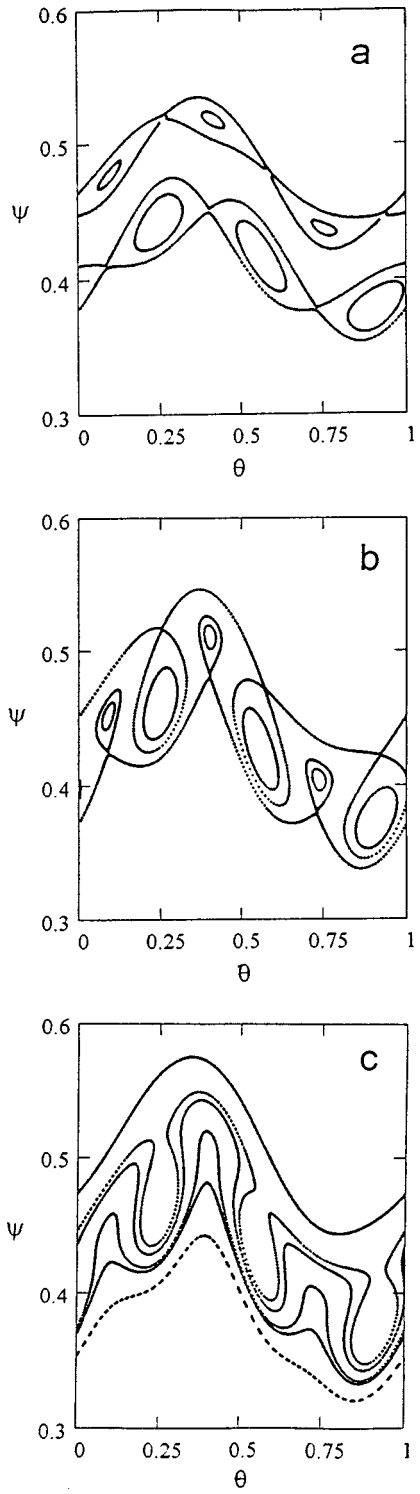

FIG. 14. Collision of $\omega = \frac{2}{3}$ islands by passage through reconnection and bifurcation upon increasing K. $w = 0.67$ and $w_0 = 0.3333$ (both fixed). (a) Below reconnection ($K = 1.5$). (b) Between reconnection and bifurcation ($K = 2$). (c) Above bifurcation ($K = 2.15$).

the W profile are colliding. The homoclinic topology ensures the mutual ''insulation'' of the two island chains: although strongly overlapping in space, they are isolated from each other by their homoclinic separatrices. As K is further increased, the islands shrink, and finally disappear after the passage through a second critical value of K producing a

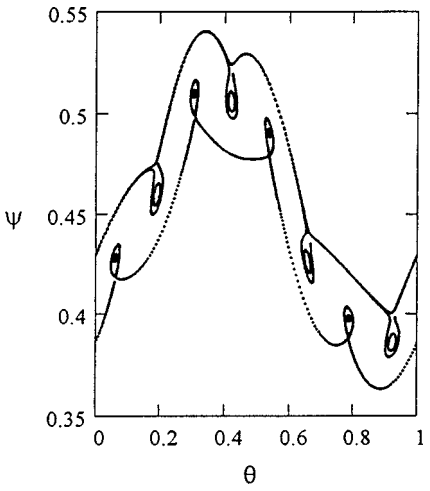

FIG. 15. Collision of $\omega=\frac{3}{4}$ islands between reconnection and bifurcation. $K=1.8$, $w=0.754$, and $w_0=0.3333$.

bifurcation [Fig. 14(c)]: there are no longer any $\omega=\frac{2}{3}$ islands left above this value of K.

An interesting case is illustrated in Fig. 15. We see here a collision of *period-4 orbits:* the process is exactly the same as for the collision of period-3 orbits illustrated in Fig. 14: starting from two neighboring four-island chains with heteroclinic topology and increasing K, a separatrix reconnection produces the homoclinic topology shown in Fig. 15, followed by the disappearance of the islands. The unusual feature is precisely that there is no difference with the period-3 case. In the standard nontwist map [Eq. (7)] studied in Refs. [18–21], there appears an essential difference between odd and even-period island chains: the latter collide by producing real dipole structures as in Fig. 12(c). This is only possible when the O points (and also the X points) of the initial neighboring island chains are aligned on the same value of θ. This is the case in Fig. 12(c) (although one of the components of the dipole is a ''ghost''). In the standard nontwist map, the even-period island chains indeed have this property (see Figs. 6 and 7 of Ref. [20], and Fig. 3 of Ref. [14]). In the revtokamap, on the other hand, the O points of neighboring islands appear to be shifted in θ with respect to each other, both for odd and even periods. The mechanism of reconnection is therefore always like in Fig. 14. We found no combination of parameters which would lead to physical dipole formation.

V. CONCLUSIONS

We have shown that a simple iterative map (*revtokamap*) can be constructed, fulfilling the minimum requirements for a representation of a magnetic field in toroidal geometry with a reversed shear configuration. It is a typical Hamiltonian nontwist map. The presence of a nonmonotonous winding number profile introduces a number of features as compared to the monotonous tokamap. In particular, there appears a ''transport barrier'' separating a robust, central region from a semiglobally chaotic edge region. This transport barrier exists even for small values of the stochasticity parameter K. On the other hand, a variety of bifurcation phenomena is exhibited in the central region, depending on the relative values of the control parameters K, w, and w_0. These result from the combination of the properties of general nontwist maps with the specific features of the revtokamap (invariance of the polar axis). It would be very interesting to envisage an experimental test of these unusual bifurcation and reconnection phenomena in a real tokamak.

Many more properties of the tokamap and of the revtokamap will be studied in forthcoming works. These include questions such as the dependence on the parameters of various physical properties, similarity and scaling properties. Last but not least, we intend to introduce charged particles into this magnetic field and study the transport of particles and heat in a partially chaotic tokamak configuration. This problem, which is very poorly understood, is of crucial importance for fusion physics.

ACKNOWLEDGMENTS

Fruitful discussions with Dr. M. Vlad, Dr. F. Spineanu, Dr. S. Abdullaev, Dr. K. Spatschek, Dr. H. P. Breuer, Dr. B. Weyssow, and Dr. J. Misguich are gratefully acknowledged.

[1] R. Balescu, M. Vlad, and F. Spineanu, Phys. Rev. E (to be published).
[2] H. Goldstein, *Classical Mechanics*, 2nd ed. (Addison-Wesley, New York, 1980).
[3] J. L. McCauley, *Classical Dynamics* (Cambridge University Press, Cambridge, 1997).
[4] C. Kessel, J. Manickam, G. Rewoldt, and W. M. Tang, Phys. Rev. Lett. **72**, 1212 (1994).
[5] F. M. Levinton, M. C. Zarnstorff, S. H. Batha, M. Bell, R. E. Bell, R. V. Budny, C. Bush, Z. Chang, E. Fredrickson, A. Janos, J. Manickam, A. Ramsey, S. A. Sabbagh, G. L. Schmidt, E. J. Synakowski, and G. I. Taylor, Phys. Rev. Lett. **75**, 4417 (1995).
[6] E. J. Strait, L. L. Lao, M. E. Mauel, B. W. Rice, T. S. Taylor, K. H. Burrell, M. S. Chu, E. A. Lazarus, T. H. Osborne, S. J. Thompson, and A. D. Turnbull, Phys. Rev. Lett. **75**, 4421 (1995).
[7] V. V. Yankov and J. Nycander, Comments Plasma Phys. Control. Fusion **18**, 1 (1997).
[8] K. H. Burrell, Phys. Plasmas **4**, 1499 (1997).
[9] C. M. Greenfield, D. P. Schissel, B. W. Stallard, E. A. Lazarus, G. A. Navratil, K. H. Burrell, T. A. Casper, J. C. DeBoo, E. J. Doyle, R. J. Fonck, C. B. Forest, P. Gohil, R. J. Groebner, M. Jakubowski, L. L. Lao, M. Murakami, C. C. Petty, C. L. Rettig, T. L. Rhodes, B. W. Rice, H. E. St. John, G. M. Staebler, E. J. Strait, T. S. Taylor, A. D. Turnbull, K. L. Tritz, R. E. Waltz, and the DIII-D Team, Phys. Plasmas **4**, 1596 (1997).
[10] G. Hu and W. Horton, Phys. Plasmas **4**, 3262 (1997).
[11] S. Ishida *et al.*, Phys. Rev. Lett. **79**, 3917 (1997).
[12] Y. Koide, K. H. Burrell, B. W. Rice, and T. Fujita, Plasma Phys. Controlled Fusion **40**, 97 (1998).
[13] J. Manickam, M. S. Chance, S. C. Jardin, C. Kessel, D. Monticello, N. Pomphrey, A. Reiman, C. Wang, and L. E. Zakharov, Phys. Plasmas **1**, 1601 (1994).
[14] J. E. Howard and S. M. Hohs, Phys. Rev. A **29**, 418 (1984).
[15] H. P. Breuer, K. Dietz, and M. Holthaus, Physica D **46**, 317 (1990).

[16] S. S. Abdullaev, Chaos **4**, 569 (1994).
[17] S. M. Soskin, Phys. Rev. E **50**, R44 (1994).
[18] D. del-Castillo-Negrete and P. J. Morrison, Phys. Fluids A **5**, 948 (1993).
[19] D. del-Castillo-Negrete, Ph.D. thesis, University of Texas at Austin, 1994.
[20] D. del-Castillo-Negrete, J. M. Greene, and P. J. Morrison, Physica D **91**, 1 (1996).
[21] D. del-Castillo-Negrete, J. M. Greene, and P. J. Morrison, Physica D **100**, 311 (1997).
[22] J. M. Greene, J. Math. Phys. **20**, 1183 (1979).
[23] A. J. Lichtenberg and M. A. Lieberman, *Regular and Stochastic Motion* (Springer, Berlin, 1983).
[24] L. E. Reichl, *The Transition to Chaos* (Springer, Berlin, 1992).
[25] E. Ott, *Chaos in Dynamical Systems* (Cambridge University Press, Cambridge, 1993).